ACS NANO

www.acsnano.org

ARTICLE

Introducing Overlapping Grain Boundaries in Chemical Vapor Deposited Hexagonal Boron Nitride Monolayer Films

Bernhard C. Bayer,*[,†] Sabina Caneva,[‡] Timothy J. Pennycook,[†] Jani Kotakoski,[†] Clemens Mangler,[†] Stephan Hofmann,[‡] and Jannik C. Meyer[†]

[†]Faculty of Physics, University of Vienna, Boltzmanngasse 5, A-1090 Vienna, Austria

[‡]Department of Engineering, University of Cambridge, 9 J.J. Thomson Avenue, CB3 0FA, Cambridge, U.K.

Supporting Information

ABSTRACT: **We demonstrate the growth of overlapping grain boundaries in continuous, polycrystalline hexagonal boron nitride (h-BN) monolayer films *via* scalable catalytic chemical vapor deposition. Unlike the commonly reported atomically stitched grain boundaries, these overlapping grain boundaries do not consist of defect lines within the monolayer films but are composed of self-sealing bilayer regions of limited width. We characterize this overlapping h-BN grain boundary structure in detail by complementary (scanning) transmission electron microscopy techniques and propose a catalytic growth mechanism linked to the subsurface/bulk of the process catalyst and its boron and nitrogen solubilities. Our data suggest that the overlapping grain boundaries are comparatively resilient against deleterious pinhole formation associated with grain boundary defect lines and thus may reduce detrimental breakdown effects when polycrystalline h-BN monolayer films are used as ultrathin dielectrics, barrier layers, or separation membranes.**

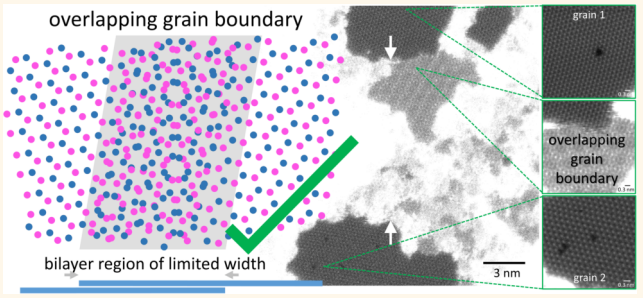

KEYWORDS: *hexagonal boron nitride, grain boundary, chemical vapor deposition, aberration-corrected scanning transmission electron microscopy, 2D materials*

Hexagonal boron nitride (h-BN) is a two-dimensional (2D) insulator with a wide application profile,[1] including its use as an ultimately thin dielectric in electronics,[2,3] a tunnel barrier in spintronics,[4,5] an encapsulation and barrier layer in electronics and metallurgy,[6] and a suspended separation membrane in nanofluidics.[7,8] All these applications require scalable manufacturing of h-BN films, whereby in particular pinhole-free continuous h-BN films of controlled layer number are desired. Catalytic chemical vapor deposition (CVD) has emerged as a promising technique to achieve growth of continuous h-BN films, including exclusive monolayer growth.[9−21] CVD h-BN films are typically polycrystalline, and control of their microstructure, in particular grain boundary (GB) structure, is important for many applications. Current literature reports the nature of the as-grown GBs in h-BN as atomically stitched, composed of defect lines within a h-BN monolayer (Figure 1a).[22−34] Preferential pinhole formation is reported at such atomically stitched GBs,[30] and due to their structure, they are intrinsically prone to electrical breakdown,[35,36] chemical attack, or mechanical failure,[26,34] all of which may render monolayer h-BN films ineffective in their envisaged applications as an ultrathin dielectric, barrier layer, or separation membrane. Recent reports on 2D materials other than h-BN however suggest the possibility to form a different type of GB, namely, overlapping GBs, where two merging 2D monolayer grains form a bilayer region of limited width at the GB instead of a defect line within the monolayer.[37−40] Overlapping GBs remain unexplored for h-BN films thus far.

Here we show using complementary (scanning) transmission electron microscopy ((S)TEM) techniques[41,42] that GBs in monolayer h-BN films grown by scalable catalytic CVD not only can be atomically stitched but can indeed also be overlapping in nature. We confirm that in overlapping GBs in h-BN monolayer films two h-BN monolayer grains merge *via* the self-sealing formation of a turbostratic bilayer region of limited width and thereby without formation of a defect line within the monolayer (Figure 1b). We characterize this overlapping GB structure in detail, identify catalytic CVD conditions that result in such GB structure, and propose

Received: December 12, 2016
Accepted: April 14, 2017
Published: April 14, 2017

DOI: 10.1021/acsnano.6b08315
ACS Nano 2017, 11, 4521−4527

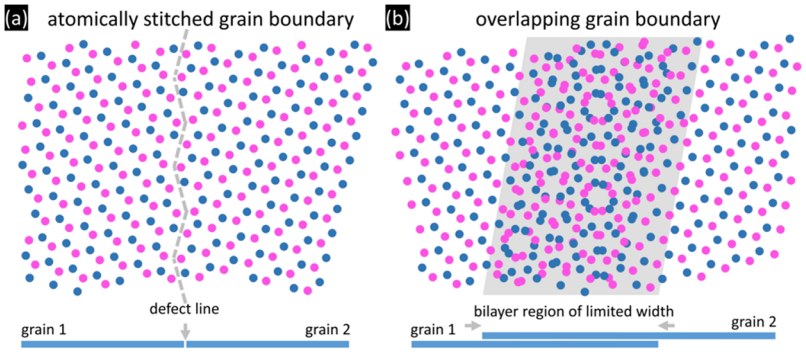

Figure 1. Illustrations (top: plan view, bottom: side view) of GB types in h-BN: (a) *Atomically stitched* GB formed by a chemically bonded interface between two grains within the h-BN monolayer, mediated by defect/dislocation lines (after ref 33). (b) *Overlapping* GB that has a van-der-Waals-type interface where two monolayer h-BN grains merge *via* a turbostratically stacked bilayer region of limited width.

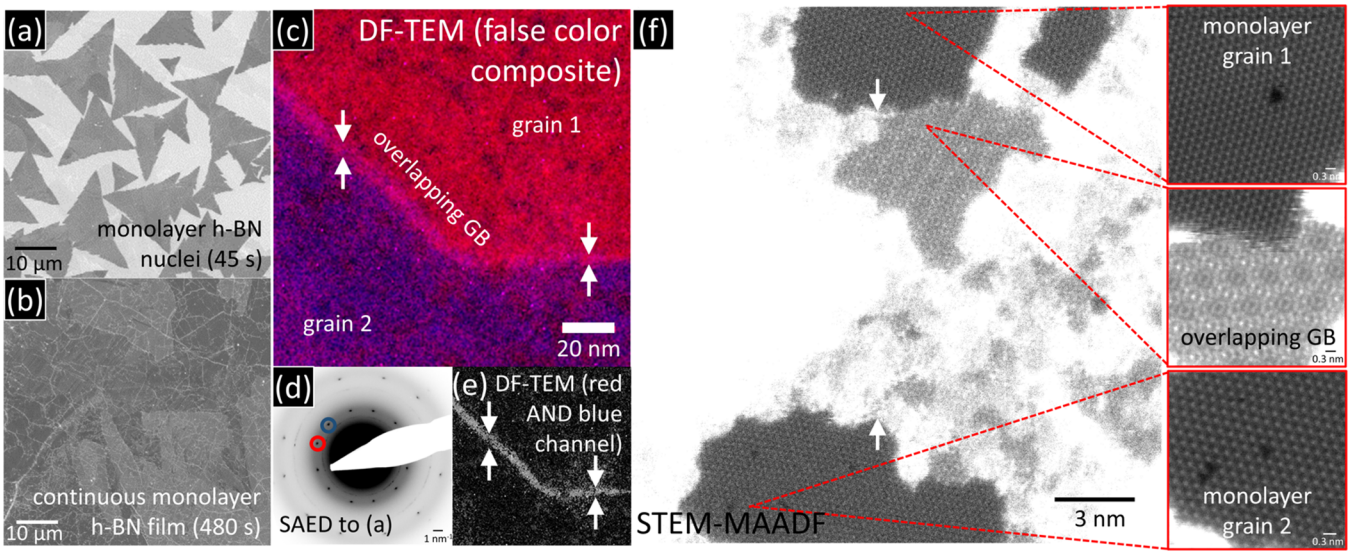

Figure 2. (a, b) SEM micrographs of h-BN growth on an Fe catalyst after NH_3 pretreatment (4 mbar) in the nucleation stage (a, borazine 45 s) and after film closure (b, borazine 480 s). (c) False-colored DF-TEM composite image of a GB in the closed h-BN film from (b), after release from the catalyst.[43−45] (d) SAED pattern corresponding to (c) with the reflections used for (c) circled in corresponding colors. (e) Overlay of the DF-TEM data from (c) after intensity thresholding and processing *via* a Boolean AND function. See Supporting Figure S1 for raw data of (a)−(e). (f) STEM image of a GB corresponding to (c)−(e) taken with a medium angle annular dark field (MAADF) detector. Insets show the indicated regions at higher magnification (and double Gaussian[42] filtered). The overlapping GB is partly covered by hydrocarbon adsorbates (bright contrast). Point defects in the h-BN monolayers are from electron beam induced damage during STEM imaging.[50,51] Supporting Figure S2 plots raw, high angle annular dark field (HAADF) and Fourier transform (FT) data of (f). Lattice distances, intensity ratios of N/B sites,[42] and layer-by-layer sputtering confirm that in (f) two monolayer h-BN grains merge in a bilayered overlapping GB (Supporting Figure S3).

possible underlying catalytic growth mechanisms. Our data suggest that overlapping GBs are comparatively resilient against detrimental pinhole formation, as evolving defects in one layer are sealed by the second layer. Thus, overlapping GBs may be technologically advantageous for the many h-BN applications for which continuous pinhole-free h-BN monolayers are key. We aim at expanding the understanding of GB formation and control in heteroelemental 2D materials such as h-BN, which directly links to their properties and various application profiles.

RESULTS AND DISCUSSION

We adopt a recently reported[18] monolayer h-BN film CVD protocol in which the employed polycrystalline Fe catalyst foils are pretreated in ammonia gas (NH_3, 4 mbar) before h-BN growth (~900 °C) by exposure to borazine ($B_3N_3H_6$, ~6 × 10^{-4} mbar) vapor. Figure 2a,b shows scanning electron micrographs (SEM) of the resulting monolayer h-BN films on the Fe catalyst in their nucleation stage (a) and after closure into a continuous h-BN monolayer film (b). To elucidate the GB structure of the closed h-BN films, we transfer[43−45] the h-BN from the Fe catalyst onto TEM grids and study the as-suspended h-BN films using dark-field (DF) and bright-field (BF) TEM (80 kV, including selected area electron diffraction (SAED))[41] and aberration-corrected STEM (60 kV).[42]

Figure 2c shows a false color coded composite of DF-TEM images across a GB in the closed h-BN film from Figure 2b, where the DF-TEM image from one h-BN monolayer grain (red, taken *via* the red circled reflection in the SAED pattern in Figure 2d) is overlaid onto the DF-TEM image of a second neighboring h-BN monolayer grain (blue, blue circled reflection in Figure 2d). Notably, along the boundary between the two merging grains a pink region of ~5 nm width (highlighted by white arrows) is visible in Figure 2c, in which the two h-BN

DOI: 10.1021/acsnano.6b08315
ACS Nano 2017, 11, 4521−4527

grains apparently *overlap*. This impression of an overlapping region along the GB is further corroborated by plotting the Boolean AND signal of both DF-TEM images in Figure 2e. Our DF-TEM data thereby suggest that GBs in our h-BN films are not of the commonly reported[22−30] atomically stitched type but instead that grains merge in an overlapping region of limited width *i.e., via* an *overlapping* GB. The two here depicted merging grains have a relative misorientation of ∼26° as derived from the SAED in Figure 2d, implying that the small width bilayer region is turbostratically stacked.[10,46−49]

The existence of overlapping GBs in our films is further confirmed at atomic resolution by the STEM image in Figure 2f. Consistent with the DF-TEM, the STEM image clearly shows that one monolayer h-BN grain (top, inset) merges with the second monolayer grain (bottom, inset) in a bilayer h-BN region of ∼10 nm width (middle, inset). Because of the in-plane misorientation between the two merging h-BN grains, the overlapping bilayer region exhibits a Moiré pattern, consistent with the SAED in Figure 2d. We find a range of ∼5−15 nm for the overlap width for other imaged GB regions for these CVD conditions.

Our data indicate that, unlike in the normally reported atomically stitched GBs,[22−30] in our overlapping GBs no defect lines are formed within the h-BN monolayers when two h-BN nuclei impinge upon each other during extended growth. Instead, the h-BN layer terminations of each grain are placed on top/under an intact second h-BN monolayer, which suggests that the formation of GB-associated pinholes may be mitigated in the overlapping GBs.

This relative resilience of the overlapping GBs against pinhole formation is indeed qualitatively corroborated by the STEM observation of electron beam induced sputtering of an h-BN film in Figure 3, when taking the resilience against electron beam induced hole formation as a proxy for pinhole formation: In Figure 3 we observe layer-by-layer sputtering in an h-BN monolayer film, comparing the monolayer basal plane (Figure 3a) and an overlapping GB (Figure 3b).[50] Importantly, under continuous electron beam exposure several extended pinholes to vacuum are readily formed in the monolayer h-BN region. This is in stark contrast to the bilayer overlapping GB region, where only point defects in one layer are formed but an intact second layer remains; that is, damage to the film is comparatively reduced in the overlapping GB region. This underscores that, in contrast to typically reported atomically stitched GBs where sputtering occurs preferentially on the weakly bonded defect lines rather than in the monolayer basal planes,[30] in our h-BN films it is easier to open a pinhole to vacuum in the basal plane of the constituent h-BN grains than in the self-sealing overlapping GB region. This indicates that in our h-BN films the intrinsic properties of the h-BN monolayer lattice rather than GB-associated defect lines determine resistance against pinhole formation.

We find no clear preferential orientation of the initial h-BN nuclei with respect to the underlying polycrystalline Fe catalyst for our growth conditions (Figure 2a).[18] This implies that the misorientation angles and distances between merging h-BN grains are not epitaxially fixed by the Fe catalyst for these CVD conditions but are rather of random nature. In line with this we find no clear rotational misalignment dependence in our overlapping GBs. Within the examined DF-TEM data set/samples overlapping GBs were the predominant type of GB, although this does not exclude the possibility that to a lesser degree also atomically stitched GBs may arise for these CVD

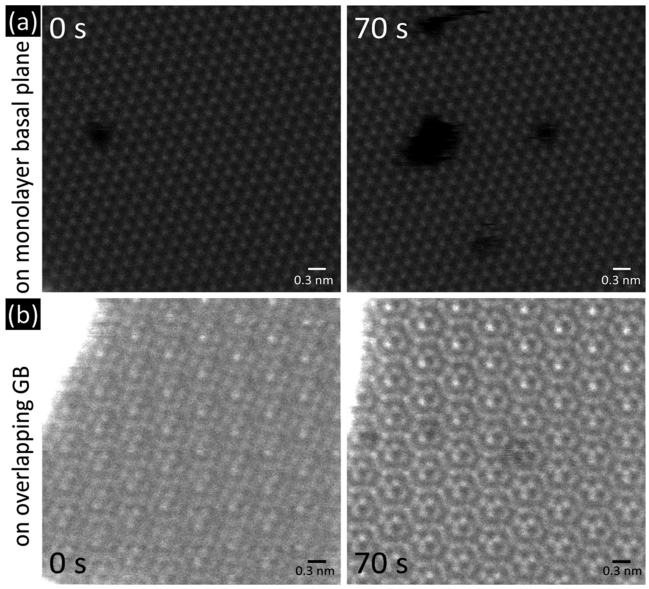

Figure 3. Double Gaussian filtered[42] MAADF STEM images of (a) a monolayer h-BN region and (b) a bilayer region in an overlapping GB (∼21° misorientation angle, see FT in Supporting Figure S4) in a monolayer h-BN film. The left images in (a) and (b) show the respective first image taken at this magnification (0 s), after which the electron beam was scanned continuously for 70 s over the shown area. The respective right images in (a) and (b) were then acquired after these 70 s of continuous beam exposure. The sputtering series clearly displays that at these imaging conditions in the monolayer region several holes to vacuum are readily opened (where typically even within the first acquisition frame a first defect emerges that widens in the subsequent 70 s beam exposure, as also seen here). In contrast, in the bilayer region in the overlapping GB no hole to vacuum has been opened by the 70 s beam exposure, but only indications for sputter-induced point defects in one layer are observed, while the second layer remained intact. This shows that the h-BN monolayer basal plane itself is more susceptible to electron beam induced pinhole formation than the bilayer region in the overlapping GB.

conditions (although such were not observed). Similar to normal atomically stitched GBs,[41] also the overlapping GBs preferentially attract contamination from adventitious hydrocarbon adsorption (Figure 2f), which is related to the increased chemical reactivity/dangling bonds at the edges of the overlapping regions. In contrast to atomically stitched GBs, in the overlapping GBs these reactive sites are however placed on top of a second *intact* h-BN layer.

A key question arising from the observation of the overlapping GBs is which factors enable their growth. We have previously shown[18] that with the here employed Fe catalyst foils the pretreatment stage with NH_3 is key to facilitate monolayer h-BN growth instead of uncontrolled multilayer formation. This is due to Fe having finite solubilities and diffusivities for B and N, which leads to dissolution of both B and N into the Fe catalyst bulk during borazine exposure when an N-free pretreatment gas, such as H_2, is used. For H_2 pretreatment, this B/N dissolution before h-BN nucleation results in multilayer h-BN pyramids without film closure (Supporting Figure S5) from a mixed growth mode of isothermal multilayer h-BN surface growth and precipitation growth of additional h-BN layers upon cooling (driven out of the catalyst bulk due to the strongly decreasing B/N solubilities in Fe with cooling).[18,52] Pretreating in a N-containing gas[53]

DOI: 10.1021/acsnano.6b08315
ACS Nano 2017, 11, 4521−4527

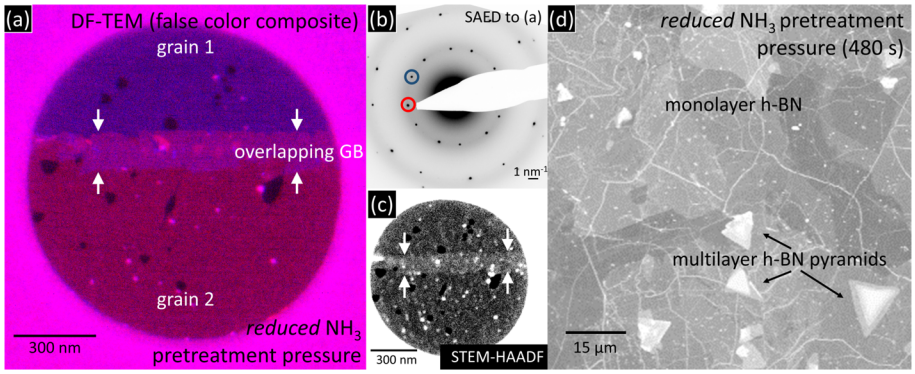

Figure 4. (a) False-colored DF-TEM composite image of a comparably wider overlapping GB in a closed h-BN film from NH_3 pretreatment at *reduced* pressure (3 mbar). The sawtoothed shape of the edge of the blue color-coded grain is typical for diffusion effects during growth of high-quality monolayer h-BN grains.[14,18,55] The formation of holes in the h-BN film is ascribed to film transfer and/or TEM imaging, where notably holes are predominantly located within the monolayer grains but not within the overlapping GB region, consistent with Figure 3. (b) SAED pattern corresponding to (a) with the reflections used for (a) circled in corresponding colors. See Supporting Figure S6 for raw data for (a) and (b). (c) STEM image of the GB in (a). (d) SEM micrograph of the h-BN film from (a) on its Fe catalyst foil.

such as NH_3 was found to prefill the catalyst bulk with N, thus hindering uptake of B (or further N) into the catalyst bulk upon the subsequent borazine exposure and thus forcing an isothermal surface growth mode of exclusive monolayer h-BN growth (Figure 2a,b),[18] as here employed. Our now here presented observation of overlapping GBs with bilayer regions of limited width in these monolayer h-BN films in turn suggests that this prefill with N is not complete but leaves the possibility for a small remaining contribution from the catalyst subsurface/bulk toward the growth of the small bilayer region in the overlapping GB. We suggest that the growth of this limited width bilayer occurs isothermally when two monolayer h-BN grains extend toward each other, and then, upon impingement, one layer grows for a limited width underneath the other layer fed *via* the only partly deactivated catalyst subsurface/bulk, analogous to subsequent layer growth from below in graphene CVD.[54] We, however, note that, alternatively, also precipitation of B and N from the limited reservoir in the catalyst subsurface/bulk upon cooling may add laterally to an existing h-BN monolayer near the junction of two not yet merged monolayer grains, resulting in growth of one layer under the other and thus an overlapping GB bilayer region of limited width. While without *in situ* experimentation the exact growth kinetics remain unknown, both scenarios imply that for controlling the formation of overlapping GBs the catalyst subsurface/bulk contribution to growth is key.

To test this hypothesis, we present in Figure 4 the effect of *reducing* the NH_3 pretreatment pressure. Such a reduced NH_3 pretreatment pressure should result in even less complete catalyst prefilling with N and thus an increased catalyst subsurface/bulk contribution to growth, be it isothermal or from precipitation upon cooling. Figure 4a,b show a false color composite DF-TEM image, and Figure 4c shows a thickness-sensitive STEM image of a typical GB in a continuous h-BN monolayer film from NH_3 pretreatment at a *reduced* NH_3 pressure of 3 mbar (instead of 4 mbar as in Figure 2). Consistent with our data above, both DF-TEM and STEM data in Figure 4 clearly indicate the formation of an overlapping GB at the border between the two neighboring h-BN grains (misorientation angle ~25°). Notably, however, the reduced NH_3 pretreatment pressure has resulted in a significant *increase* in the width of the overlapping region in the GB to ~100 nm in Figure 4 (with a range of ~20−110 nm for other imaged GBs on this reduced NH_3 pretreatment pressure sample, as compared to only ~5−15 nm in Figure 2). This increased width of the overlapping region is in line with our hypothesis above that a reduced N prefilling results in an increased catalyst subsurface/bulk contribution to h-BN growth, which in turn facilitates the formation of the wider overlapping GBs. Additional characterization of the h-BN films from NH_3 pretreatment at reduced pressure further corroborates this increased contribution of the catalyst subsurface/bulk to growth, as besides the predominant monolayer regions in these samples also isolated multilayer pyramids on/under the continuous monolayer regions are observed (Figure 4d). In contrast, no such multilayer pyramids were found in the exclusive monolayer films from the higher NH_3 pretreatment pressure in Figure 2. This suggests that by controlling the level of prefilling of the catalyst subsurface/bulk the width of the overlapping GBs in the h-BN films can be controlled. This control is however coupled to a transition from exclusive monolayer film growth (high NH_3 pretreatment pressure, Figure 2) to mixed monolayer/multilayer film (reduced NH_3 pretreatment pressure, Figure 4) and finally to growth of only isolated multilayer h-BN pyramids (H_2 pretreatment, *i.e.*, no N prefilling, Supporting Figure S5). We emphasize that the suggested increased subsurface/bulk contribution to h-BN from NH_3 pretreatment at reduced pressure is also consistent with our previous *in situ* X-ray photoelectron spectroscopy characterization of h-BN growth.[18] The measured range of misorientation angles of grains with overlapping GBs for the reduced NH_3 pretreatment pressure conditions is ~5° to ~25°. We find no obvious correlation between overlapping region width (range of ~20−110 nm) and grain misorientation (range of 5−25°) angle of the overlapping GBs for these conditions. This further reaffirms that the NH_3 pretreatment pressure is the determining factor for the overlapping GB growth, while the h-BN grain misorientation angle in the turbostratic bilayer overlap regions appears to be less important under our conditions. This is also exemplified when considering that in Figures 2 and 3 the high 4 mbar pressure NH_3 pretreatment yields only a few nanometer overlap (up to 15 nm) for misorientations of ~21° to ~26°, while for a misorientation angle in the same range (~25°) the reduced 3 mbar NH_3 pretreatment yields up to 110 nm overlap in Figure 4.

DOI: 10.1021/acsnano.6b08315
ACS Nano 2017, 11, 4521−4527

Despite h-BN's wide application potential, only few experimental studies on GBs in monolayer h-BN are available to date,[22−30] with particularly few at atomic resolution.[23−25] Experimental verification of proposed GB types in monolayer h-BN therefore remains critically lacking.[56] Among the experimental studies only atomically stitched GBs[22−30] were observed in monolayer h-BN, and also theoretical work has so far only focused on atomically stitched GBs.[31−34] In contrast, our work here highlights that GBs in h-BN monolayer films can also be overlapping in nature, demanding further consideration.

In the context of other 2D materials, overlapping GBs have been previously reported for CVD graphene[37,38] and CVD MoS_2.[39,40] On a related note, overlapping *heterostructure* junction formation between h-BN and graphene has been previously observed, where, in agreement with our data here, the type of heterojunction was a function of CVD processing conditions.[57] Similarly, overlapping heterostructure junctions have been recently found between GaSe/$MoSe_2$,[58] highlighting the generic but thus far often overlooked nature of the here reported van-der-Waals-type overlapping GBs in 2D materials.

It is noteworthy that among the few available reports[22−30] on GBs in monolayer h-BN (where only atomically stitched GBs were reported) mostly Cu has been investigated as a polycrystalline metallic catalyst for scalable catalytic CVD conditions.[24−28,30] Unlike Fe, which has finite solubilities for both B and N, Cu has a finite solubility for B but negligible solubility for N.[11] This intrinsically (*i.e.*, without the requirement for catalyst prefilling) limits h-BN growth on Cu to an isothermal growth mode with an inherently restricted subsurface/bulk contribution to growth.[11] We note that, in line with our suggested subsurface/bulk-mediated growth mechanism for the overlapping GBs, this difference in B/N solubilities between Cu and Fe and the resulting inherently smaller subsurface/bulk contribution to growth on Cu may account for the absence[24−28,30] of overlapping GBs in the Cu-catalyzed h-BN monolayers.

While our data indicate that the overlapping GBs may be beneficial for avoiding pinhole formation in monolayer h-BN films, we note that such van-der-Waals-type boundaries with turbostratic stacking in the overlapping region may in turn reduce the tensile strength of a polycrystalline 2D material compared to atomically stitched GBs.[34] Particularly for h-BN, also the doubled layer number along the overlapping GBs has to be considered when the h-BN is desired as a dielectric film where a constant dielectric thickness may be key for device performance.[36] Thus, whether atomically stitched or overlapping GBs are preferable will partly depend on the exact application requirements. Our introduction of the overlapping GB type in h-BN monolayer films however critically adds to the available toolbox for h-BN film microstructure control.

CONCLUSIONS

In summary, we have shown that overlapping GBs can be introduced into CVD h-BN monolayer films by controlling subsurface/bulk growth contributions *via* rational catalyst and pretreatment choice. In contrast to the commonly reported atomically stitched GBs these overlapping GBs are not formed by a defect line within the monolayer but comprise a self-sealing bilayer region of limited width. Our data suggest that overlapping GBs are comparatively resilient against detrimental pinhole formation. Thus, the overlapping GBs may mitigate failure from GB-associated pinholes when polycrystalline h-BN monolayer films are utilized as ultrathin dielectrics, barrier layers, or separation membranes. Our results here aim at expanding the understanding of GB formation in h-BN CVD and possible engineering to tailor h-BN film morphology for application needs.

METHODS

For growth of the monolayer h-BN films we adopt a recently reported CVD protocol,[18] using commercial Fe foils (0.1 mm, Alfa Aesar, 99.99% purity) as catalyst and a customized Aixtron BM3 as cold-wall reactor (base pressure 1×10^{-6} mbar). After pumping to base pressure, we pretreat the catalyst in 3 (reduced pressure) or 4 (high pressure) mbar of NH_3 (or, for reference, 4 mbar of H_2) while ramping to a temperature of ∼900 °C. After reaching ∼900 °C, the pretreatment gas is removed and h-BN growth is initiated by dosing borazine vapor ($B_3N_3H_6$, 6×10^{-4} mbar) into the reactor. For a closed film from NH_3 pretreatment the borazine exposure time was 480 s, while shorter exposure times (45 s) arrested h-BN growth in the nucleation stage. After exposure to borazine the reactor was pumped to base pressure and the heater was switched off, leaving the samples to cool naturally (initial cooling rate ∼300 °C/min) in a vacuum. For (S)TEM characterization the h-BN films were transferred *via* the electrochemical bubbling method[43] onto holey carbon TEM grids with regular hole arrays (Quantifoil, ∼1 μm hole diameters). BF- and DF-TEM[41] and SAED of such transferred samples were measured in a Philips CM200 TEM at 80 kV electron acceleration voltage. Atomically resolved STEM was measured in an aberration-corrected Nion UltraSTEM 100 at an electron acceleration voltage of 60 kV while keeping the sample in a vacuum of $\sim 10^{-9}$ mbar, simultaneously acquiring HAADF (80 to 200 mrad) and MAADF (40 to 80 mrad) signals. Typical beam currents of ∼30 pA equate for a spot size of ∼1 $Å^2$ to typical electron dose rates directly under the beam of $\sim 5 \times 10^8$ $e^- Å^{-2} s^{-1}$, which result in average dose rates of $\sim 2 \times 10^5$ $e^- Å^{-2} s^{-1}$ for continuous scanning of a 5 nm × 5 nm area (as in Figure 3). For further details on methods see the Supporting Information.

ASSOCIATED CONTENT

Supporting Information

The Supporting Information is available free of charge on the ACS Publications website at DOI: 10.1021/acsnano.6b08315.

Detailed description of experimental methods and additional TEM, STEM, and SEM data (PDF)

AUTHOR INFORMATION

Corresponding Author

*E-mail: bernhard.bayer@univie.ac.at.

ORCID

Bernhard C. Bayer: 0000-0002-4829-3207
Jani Kotakoski: 0000-0002-1301-5266
Stephan Hofmann: 0000-0001-6375-1459
Jannik C. Meyer: 0000-0003-4023-0778

Notes

The authors declare no competing financial interest.

ACKNOWLEDGMENTS

We acknowledge funding from the European Union's Horizon 2020 research and innovation program under the Marie Skłodowska-Curie Grant Agreements 656214-2DInterFOX (B.C.B.) and 655760-DIGIPHASE (T.J.P.). S.C. acknowledges a doctoral training award from the EPSRC, UK. We also acknowledge the Wiener Wissenschafts, Forschungs- und Technologiefond (WWTF, MA14-009, J.K.), the European Research Council (ERC, 279342, S.H.), the EPSRC, UK (EP/K016636/1, S.H.), and the Austrian Science Fund (FWF, P25721-N20, J.C.M.).

DOI: 10.1021/acsnano.6b08315
ACS Nano 2017, 11, 4521−4527

REFERENCES

(1) Pakdel, A.; Bando, Y.; Golberg, D. Nano Boron Nitride Flatland. *Chem. Soc. Rev.* **2014**, *43*, 934−959.

(2) Dean, C. R.; Young, A. F.; Meric, I.; Lee, C.; Wang, L.; Sorgenfrei, S.; Watanabe, K.; Taniguchi, T.; Kim, P.; Shepard, K.; Hone, J. Boron Nitride Substrates for High-Quality Graphene Electronics. *Nat. Nanotechnol.* **2010**, *5*, 722−726.

(3) Pan, C.; Ji, Y.; Xiao, N.; Hui, F.; Tang, K.; Guo, Y.; Xie, X.; Puglisi, F. M.; Larcher, L.; Miranda, E.; Jiang, L.; Shi, Y.; Valov, I.; McIntyre, P. C.; Waser, R.; Lanza, M. Coexistence of Grain-Boundaries-Assisted Bipolar and Threshold Resistive Switching in Multilayer Hexagonal Boron Nitride. *Adv. Funct. Mater.* **2017**, *27*, 1604811.

(4) Fu, W.; Makk, P.; Maurand, R.; Bräuninger, M.; Schönenberger, C. Large-Scale Fabrication of BN Tunnel Barriers for Graphene Spintronics. *J. Appl. Phys.* **2014**, *116*, 74306.

(5) Piquemal-Banci, M.; Galceran, R.; Caneva, S.; Martin, M.-B.; Weatherup, R. S.; Kidambi, P. R.; Bouzehouane, K.; Xavier, S.; Anane, A.; Petroff, F.; Fert, A.; Robertson, J.; Hofmann, S.; Dlubak, B.; Seneor, P. Magnetic Tunnel Junctions with Monolayer Hexagonal Boron Nitride Tunnel Barriers. *Appl. Phys. Lett.* **2016**, *108*, 102404.

(6) Liu, Z.; Gong, Y.; Zhou, W.; Ma, L.; Yu, J.; Idrobo, J. C.; Jung, J.; MacDonald, A. H.; Vajtai, R.; Lou, J.; Ajayan, P. M. Ultrathin High-Temperature Oxidation-Resistant Coatings of Hexagonal Boron Nitride. *Nat. Commun.* **2013**, *4*, 2541.

(7) Liu, S.; Lu, B.; Zhao, Q.; Li, J.; Gao, T.; Chen, Y.; Zhang, Y.; Liu, Z.; Fan, Z.; Yang, F.; You, L.; Yu, D. Boron Nitride Nanopores: Highly Sensitive DNA Single-molecule Detectors. *Adv. Mater.* **2013**, *25*, 4549−4554.

(8) Hu, S.; Lozada-Hidalgo, M.; Wang, F. C.; Mishchenko, A.; Schedin, F.; Nair, R. R.; Hill, E. W.; Boukhvalov, D. W.; Katsnelson, M. I.; Dryfe, R. A. W.; Grigorieva, I. V.; Wu, H. A.; Geim, A. K. Proton Transport through One-Atom-Thick Crystals. *Nature* **2014**, *516*, 227−230.

(9) Kim, K. K.; Hsu, A.; Jia, X.; Kim, S. M.; Shi, Y.; Hofmann, M.; Nezich, D.; Rodriguez-Nieva, J. F.; Dresselhaus, M.; Palacios, T.; Kong, J. Synthesis of Monolayer Hexagonal Boron Nitride on Cu Foil Using Chemical Vapor Deposition. *Nano Lett.* **2011**, *12*, 161−166.

(10) Kim, C.-J.; Brown, L.; Graham, M. W.; Hovden, R.; Havener, R. W.; McEuen, P. L.; Muller, D. A.; Park, J. Stacking Order Dependent Second Harmonic Generation and Topological Defects in H-BN Bilayers. *Nano Lett.* **2013**, *13*, 5660−5665.

(11) Kidambi, P. R.; Blume, R.; Kling, J.; Wagner, J. B.; Baehtz, C.; Weatherup, R. S.; Schloegl, R.; Bayer, B. C.; Hofmann, S. *In Situ* Observations during Chemical Vapor Deposition of Hexagonal Boron Nitride on Polycrystalline Copper. *Chem. Mater.* **2014**, *26*, 6380−6392.

(12) Orlando, F.; Lacovig, P.; Omiciuolo, L.; Apostol, N. G.; Larciprete, R.; Baraldi, A.; Lizzit, S. Epitaxial Growth of a Single-Domain Hexagonal Boron Nitride Monolayer. *ACS Nano* **2014**, *8*, 12063−12070.

(13) Tay, R. Y.; Griep, M. H.; Mallick, G.; Tsang, S. H.; Singh, R. S.; Tumlin, T.; Teo, E. H. T.; Karna, S. P. Growth of Large Single-Crystalline Two-Dimensional Boron Nitride Hexagons on Electropolished Copper. *Nano Lett.* **2014**, *14*, 839−846.

(14) Caneva, S.; Weatherup, R. S.; Bayer, B. C.; Brennan, B.; Spencer, S. J.; Mingard, K.; Cabrero-Vilatela, A.; Baehtz, C.; Pollard, A. J.; Hofmann, S. Nucleation Control for Large, Single Crystalline Domains of Monolayer Hexagonal Boron Nitride *via* Si-Doped Fe Catalysts. *Nano Lett.* **2015**, *15*, 1867−1875.

(15) Wood, G. E.; Marsden, A. J.; Mudd, J. J.; Walker, M.; Asensio, M.; Avila, J.; Chen, K.; Bell, G. R.; Wilson, N. R. Van Der Waals Epitaxy of Monolayer Hexagonal Boron Nitride on Copper Foil: Growth, Crystallography and Electronic Band Structure. *2D Mater.* **2015**, *2*, 025003.

(16) Stehle, Y.; Meyer, H. M., III; Unocic, R. R.; Kidder, M.; Polizos, G.; Datskos, P. G.; Jackson, R.; Smirnov, S. N.; Vlassiouk, I. V. Synthesis of Hexagonal Boron Nitride Monolayer: Control of Nucleation and Crystal Morphology. *Chem. Mater.* **2015**, *27*, 8041−8047.

(17) Lu, G.; Wu, T.; Yuan, Q.; Wang, H.; Wang, H.; Ding, F.; Xie, X.; Jiang, M. Synthesis of Large Single-Crystal Hexagonal Boron Nitride Grains on Cu−Ni Alloy. *Nat. Commun.* **2015**, *6*, 6160.

(18) Caneva, S.; Weatherup, R. S.; Bayer, B. C.; Blume, R.; Cabrero-Vilatela, A.; Braeuninger-Weimer, P.; Martin, M.-B.; Wang, R.; Baehtz, C.; Schloegl, R.; Meyer, J. C.; Hofmann, S. Controlling Catalyst Bulk Reservoir Effects for Monolayer Hexagonal Boron Nitride CVD. *Nano Lett.* **2016**, *16*, 1250−1261.

(19) Xu, Z.; Tian, H.; Khanaki, A.; Zheng, R.; Suja, M.; Liu, J. Large-Area Growth of Multi-Layer Hexagonal Boron Nitride on Polished Cobalt Foils by Plasma-Assisted Molecular Beam Epitaxy. *Sci. Rep.* **2017**, *7*, 43100.

(20) Uchida, Y.; Iwaizako, T.; Mizuno, S.; Tsuji, M.; Ago, H. Epitaxial Chemical Vapour Deposition Growth of Monolayer Hexagonal Boron Nitride on Cu (111)/sapphire Substrate. *Phys. Chem. Chem. Phys.* **2017**, *19*, 8230−8235.

(21) Meng, J.; Zhang, X.; Wang, Y.; Yin, Z.; Liu, H.; Xia, J.; Wang, H.; You, J.; Jin, P.; Wang, D.; Meng, X.-M. Aligned Growth of Millimeter-Size Hexagonal Boron Nitride Single-Crystal Domains on Epitaxial Nickel Thin Film. *Small* **2017**, 1604179.

(22) Auwärter, W.; Muntwiler, M.; Osterwalder, J.; Greber, T. Defect Lines and Two-Domain Structure of Hexagonal Boron Nitride Films on Ni(1 1 1). *Surf. Sci.* **2003**, *545*, L735−L740.

(23) Lu, J.; Yeo, P. S. E.; Zheng, Y.; Xu, H.; Gan, C. K.; Sullivan, M. B.; Castro Neto, A. H.; Loh, K. P. Step Flow *Versus* Mosaic Film Growth in Hexagonal Boron Nitride. *J. Am. Chem. Soc.* **2013**, *135*, 2368−2373.

(24) Gibb, A. L.; Alem, N.; Chen, J.-H.; Erickson, K. J.; Ciston, J.; Gautam, A.; Linck, M.; Zettl, A. Atomic Resolution Imaging of Grain Boundary Defects in Monolayer Chemical Vapor Deposition-Grown Hexagonal Boron Nitride. *J. Am. Chem. Soc.* **2013**, *135*, 6758−6761.

(25) Li, Q.; Zou, X.; Liu, M.; Sun, J.; Gao, Y.; Qi, Y.; Zhou, X.; Yakobson, B. I.; Zhang, Y.; Liu, Z. Grain Boundary Structures and Electronic Properties of Hexagonal Boron Nitride on Cu(111). *Nano Lett.* **2015**, *15*, 5804−5810.

(26) Yin, J.; Yu, J.; Li, X.; Li, J.; Zhou, J.; Zhang, Z.; Guo, W. Large Single-Crystal Hexagonal Boron Nitride Monolayer Domains with Controlled Morphology and Straight Merging Boundaries. *Small* **2015**, *11*, 4497−4502.

(27) Song, X.; Gao, J.; Nie, Y.; Gao, T.; Sun, J.; Ma, D.; Li, Q.; Chen, Y.; Jin, C.; Bachmatiuk, A.; Rümmeli, M. H.; Ding, F.; Zhang, Y.; Liu, Z. Chemical Vapor Deposition Growth of Large-Scale Hexagonal Boron Nitride with Controllable Orientation. *Nano Res.* **2015**, *8*, 3164−3176.

(28) Wu, Q.; Park, J.-H.; Park, S.; Jung, S. J.; Suh, H.; Park, N.; Wongwiriyapan, W.; Lee, S.; Lee, Y. H.; Song, Y. J. Single Crystalline Film of Hexagonal Boron Nitride Atomic Monolayer by Controlling Nucleation Seeds and Domains. *Sci. Rep.* **2015**, *5*, 16159.

(29) Yin, J.; Liu, X.; Lu, W.; Li, J.; Cao, Y.; Li, Y.; Xu, Y.; Li, X.; Zhou, J.; Jin, C.; Guo, W. Aligned Growth of Hexagonal Boron Nitride Monolayer on Germanium. *Small* **2015**, *11*, 5375−5380.

(30) Tay, R. Y.; Park, H. J.; Ryu, G. H.; Tan, D.; Tsang, S. H.; Li, H.; Liu, W.; Teo, E. H. T.; Lee, Z.; Lifshitz, Y.; Ruoff, R. S. Synthesis of Aligned Symmetrical Multifaceted Monolayer Hexagonal Boron Nitride Single Crystals on Resolidified Copper. *Nanoscale* **2016**, *8*, 2434−2444.

(31) Liu, Y.; Zou, X.; Yakobson, B. I. Dislocations and Grain Boundaries in Two-Dimensional Boron Nitride. *ACS Nano* **2012**, *6*, 7053−7058.

(32) Li, X.; Wu, X.; Zeng, X. C.; Yang, J. Band-Gap Engineering *via* Tailored Line Defects in Boron-Nitride Nanoribbons, Sheets, and Nanotubes. *ACS Nano* **2012**, *6*, 4104−4112.

(33) Wang, Z. Structure and Electronic Properties of Boron Nitride Sheet with Grain Boundaries. *J. Nanopart. Res.* **2012**, *14*, 756.

(34) Ding, N.; Wu, C.-M. L.; Li, H. The Effect of Grain Boundaries on the Mechanical Properties and Failure Behavior of Hexagonal

DOI: 10.1021/acsnano.6b08315
ACS Nano 2017, 11, 4521−4527

Boron Nitride Sheets. *Phys. Chem. Chem. Phys.* **2014**, *16*, 23716−23722.
(35) Chandni, U.; Watanabe, K.; Taniguchi, T.; Eisenstein, J. Evidence for Defect-Mediated Tunneling in Hexagonal Boron Nitride-Based Junctions. *Nano Lett.* **2015**, *15*, 7329−7333.
(36) Hui, F.; Pan, C.; Shi, Y.; Ji, Y.; Grustan-Gutierrez, E.; Lanza, M. On the Use of Two Dimensional Hexagonal Boron Nitride as Dielectric. *Microelectron. Eng.* **2016**, *163*, 119−133.
(37) Tsen, A. W.; Brown, L.; Levendorf, M. P.; Ghahari, F.; Huang, P. Y.; Havener, R. W.; Ruiz-Vargas, C. S.; Muller, D. A.; Kim, P.; Park, J. Tailoring Electrical Transport Across Grain Boundaries in Polycrystalline Graphene. *Science* **2012**, *336*, 1143−1146.
(38) Robertson, A. W.; Bachmatiuk, A.; Wu, Y. A.; Schäffel, F.; Rellinghaus, B.; Büchner, B.; Rümmeli, M. H.; Warner, J. H. Atomic Structure of Interconnected Few-Layer Graphene Domains. *ACS Nano* **2011**, *5*, 6610−6618.
(39) Najmaei, S.; Liu, Z.; Zhou, W.; Zou, X.; Shi, G.; Lei, S.; Yakobson, B. I.; Idrobo, J.-C.; Ajayan, P. M.; Lou, J. Vapour Phase Growth and Grain Boundary Structure of Molybdenum Disulphide Atomic Layers. *Nat. Mater.* **2013**, *12*, 754−759.
(40) Elibol, K.; Susi, T.; O'Brien, M.; Bayer, B. C.; Pennycook, T. J.; McEvoy, N.; Duesberg, G. S.; Meyer, J. C.; Kotakoski, J. Grain Boundary-Mediated Nanopores in Molybdenum Disulfide Grown by Chemical Vapor Deposition. *Nanoscale* **2017**, *9*, 1591−1598.
(41) Huang, P. Y.; Ruiz-Vargas, C. S.; van der Zande, A. M.; Whitney, W. S.; Levendorf, M. P.; Kevek, J. W.; Garg, S.; Alden, J. S.; Hustedt, C. J.; Zhu, Y.; Park, J.; McEuen, P. L.; Muller, D. A. Grains and Grain Boundaries in Single-Layer Graphene Atomic Patchwork Quilts. *Nature* **2011**, *469*, 389−392.
(42) Krivanek, O. L.; Chisholm, M. F.; Nicolosi, V.; Pennycook, T. J.; Corbin, G. J.; Dellby, N.; Murfitt, M. F.; Own, C. S.; Szilagyi, Z. S.; Oxley, M. P.; Pantelides, S. T.; Pennycook, S. J. Atom-by-Atom Structural and Chemical Analysis by Annular Dark-Field Electron Microscopy. *Nature* **2010**, *464*, 571−574.
(43) Gao, L.; Ren, W.; Xu, H.; Jin, L.; Wang, Z.; Ma, T.; Ma, L.-P.; Zhang, Z.; Fu, Q.; Peng, L.-M.; Bao, X.; Cheng, H.-M. Repeated Growth and Bubbling Transfer of Graphene with Millimetre-Size Single-Crystal Grains Using Platinum. *Nat. Commun.* **2012**, *3*, 699.
(44) Kratzer, M.; Bayer, B. C.; Kidambi, P. R.; Matković, A.; Gajić, R.; Cabrero-Vilatela, A.; Weatherup, R. S.; Hofmann, S.; Teichert, C. Effects of Polymethylmethacrylate-Transfer Residues on the Growth of Organic Semiconductor Molecules on Chemical Vapor Deposited Graphene. *Appl. Phys. Lett.* **2015**, *106*, 103101.
(45) Elibol, K.; Bayer, B. C.; Hummel, S.; Kotakoski, J.; Argentero, G.; Meyer, J. C. Visualising the Strain Distribution in Suspended Two-Dimensional Materials under Local Deformation. *Sci. Rep.* **2016**, *6*, 28485.
(46) Sutter, P.; Lahiri, J.; Zahl, P.; Wang, B.; Sutter, E. Scalable Synthesis of Uniform Few-Layer Hexagonal Boron Nitride Dielectric Films. *Nano Lett.* **2013**, *13*, 276−281.
(47) Shmeliov, A.; Kim, J. S.; Borisenko, K. B.; Wang, P.; Okunishi, E.; Shannon, M.; Kirkland, A. I.; Nellist, P. D.; Nicolosi, V. Impurity Induced Non-Bulk Stacking in Chemically Exfoliated H-BN Nanosheets. *Nanoscale* **2013**, *5*, 2290−2294.
(48) Khan, M. H.; Casillas, G.; Mitchell, D. R.; Liu, H. K.; Jiang, L.; Huang, Z. Carbon-and Crack-Free Growth of Hexagonal Boron Nitride Nanosheets and Their Uncommon Stacking Order. *Nanoscale* **2016**, *8*, 15926−15933.
(49) Yang, Y.; Fu, Q.; Li, H.; Wei, M.; Xiao, J.; Wei, W.; Bao, X. Creating a Nanospace under an H-BN Cover for Adlayer Growth on Nickel (111). *ACS Nano* **2015**, *9*, 11589−11598.
(50) Meyer, J. C.; Chuvilin, A.; Algara-Siller, G.; Biskupek, J.; Kaiser, U. Selective Sputtering and Atomic Resolution Imaging of Atomically Thin Boron Nitride Membranes. *Nano Lett.* **2009**, *9*, 2683−2689.
(51) Kotakoski, J.; Jin, C.; Lehtinen, O.; Suenaga, K.; Krasheninnikov, A. Electron Knock-on Damage in Hexagonal Boron Nitride Monolayers. *Phys. Rev. B: Condens. Matter Mater. Phys.* **2010**, *82*, 113404.
(52) Kim, S. M.; Hsu, A.; Park, M. H.; Chae, S. H.; Yun, S. J.; Lee, J. S.; Cho, D.-H.; Fang, W.; Lee, C.; Palacios, T.; Dresselhaus, M.; Kim, K. K.; Lee, Y. H.; Kong, J. Synthesis of Large-Area Multilayer Hexagonal Boron Nitride for High Material Performance. *Nat. Commun.* **2015**, *6*, 8662.
(53) Bayer, B. C.; Baehtz, C.; Kidambi, P. R.; Weatherup, R. S.; Mangler, C.; Kotakoski, J.; Goddard, C. J. L.; Caneva, S.; Cabrero-Vilatela, A.; Meyer, J. C.; Hofmann, S. Nitrogen Controlled Iron Catalyst Phase during Carbon Nanotube Growth. *Appl. Phys. Lett.* **2014**, *105*, 143111.
(54) Weatherup, R. S.; Amara, H.; Blume, R.; Dlubak, B.; Bayer, B. C.; Diarra, M.; Bahri, M.; Cabrero-Vilatela, A.; Caneva, S.; Kidambi, P. R.; Martin, M.-B.; Deranlot, C.; Seneor, P.; Schloegl, R.; Ducastelle, F.; Bichara, C.; Hofmann, S. Interdependency of Subsurface Carbon Distribution and Graphene−Catalyst Interaction. *J. Am. Chem. Soc.* **2014**, *136*, 13698−13708.
(55) Artyukhov, V. I.; Hao, Y.; Ruoff, R. S.; Yakobson, B. I. Breaking of Symmetry in Graphene Growth on Metal Substrates. *Phys. Rev. Lett.* **2015**, *114*, 115502.
(56) Cretu, O.; Lin, Y.-C.; Suenaga, K. Evidence for Active Atomic Defects in Monolayer Hexagonal Boron Nitride: A New Mechanism of Plasticity in Two-Dimensional Materials. *Nano Lett.* **2014**, *14*, 1064−1068.
(57) Kim, S. M.; Hsu, A.; Araujo, P. T.; Lee, Y.-H.; Palacios, T.; Dresselhaus, M.; Idrobo, J.-C.; Kim, K. K.; Kong, J. Synthesis of Patched or Stacked Graphene and hBN Flakes: A Route to Hybrid Structure Discovery. *Nano Lett.* **2013**, *13*, 933−941.
(58) Li, X.; Lin, M.-W.; Lin, J.; Huang, B.; Puretzky, A. A.; Ma, C.; Wang, K.; Zhou, W.; Pantelides, S. T.; Chi, M.; Kravchenko, I.; Fowlkes, J.; Rouleau, C. M.; Geohegan, D. B.; Xiao, K. Two-Dimensional GaSe/$MoSe_2$ Misfit Bilayer Heterojunctions by van Der Waals Epitaxy. *Sci. Adv.* **2016**, *2*, e1501882.

DOI: 10.1021/acsnano.6b08315
ACS Nano 2017, 11, 4521−4527